




Cite this: *Phys. Chem. Chem. Phys.*,
2018, 20, 1051

Interfacial and thermal energy driven growth and evolution of Langmuir–Schaefer monolayers of Au-nanoparticles†

Mala Mukhopadhyay‡ and S. Hazra *

Structures of Langmuir–Schaefer (LS) monolayers of thiol-coated Au-nanoparticles (DT-AuNPs) deposited on H-terminated and OTS self-assembled Si substrates (of different hydrophobic strength and stability) and their evolution with time under ambient conditions, which plays an important role for their practical use as 2D-nanostructures over large areas, were investigated using the X-ray reflectivity technique. The strong effect of substrate surface energy (γ) on the initial structures and the competitive role of room temperature thermal energy (kT) and the change in interfacial energy ($\Delta\gamma$) at ambient conditions on the evolution and final structures of the DT-AuNP LS monolayers are evident. The strong-hydrophobic OTS-Si substrate, during transfer, seems to induce strong attraction towards hydrophobic DT-AuNPs on hydrophilic (repulsive) water to form vertically compact partially covered (with voids) monolayer structures (of perfect monolayer thickness) at low pressure and nearly covered buckled monolayer structures (of enhanced monolayer thickness) at high pressure. After transfer, the small kT -energy (in absence of repulsive water) probably fluctuates the DT-AuNPs to form vertically expanded monolayer structures, through systematic exponential growth with time. The effect is prominent for the film deposited at low pressure, where the initial film-coverage and film-thickness are low. On the other hand, the weak-hydrophobic H-Si substrate, during transfer, appears to induce optimum attraction towards DT-AuNPs to better mimic the Langmuir monolayer structures on it. After transfer, the change in the substrate surface nature, from weak-hydrophobic to weak-hydrophilic with time (*i.e.* $\Delta\gamma$ -energy, apart from the kT -energy), enhances the size of the voids and weakens the monolayer/bilayer structure to form a similar expanded monolayer structure, the thickness of which is probably optimized by the available thermal energy.

Received 25th October 2017,
Accepted 4th December 2017

DOI: 10.1039/c7cp07236h

rsc.li/pccp

1 Introduction

Low-dimensional systems or nano-objects, having sizes smaller than a certain intrinsic physical length, demonstrate properties that are sometimes completely different from the bulk ones.^{1–4} Such nano-objects can act as building blocks to form organized structures with useful electronic, optical, and magnetic properties.^{5–9} For example, thiol-capped gold nanoparticles (DT-AuNPs) form self-assembled 2D-structures,^{9–12} due to the complex balance of long-range van der Waals (vdW) attractions and short-range steric repulsion^{13–18} initiated by solvent evaporation.^{19–21} Such 2D-structures formed at air/water interfaces, known as Langmuir monolayers, can be readily transferred

onto a solid substrate using Langmuir–Blodgett (LB) and Langmuir–Schaefer (LS) techniques to grow uniform nanostructures over large areas.^{2,12,22–26} The performance of the 2D-nanostructures, which arises from the new collective phenomena related to the interparticle coupling,^{2,6–10} can strongly depend on how nanoparticles are adsorbed at the interfaces and their equilibrium position, their lateral interaction, and their 2D ordering.²⁷

The structures of such films on solid substrates are governed by the structures of the Langmuir monolayers, the monolayer–substrate interactions during transfer and their evolution with time. A hydrophilic substrate, due to its repulsive force on the DT-AuNP Langmuir monolayer (for both LB and LS depositions), can perturb and change the monolayer structure, which with time can evolve further. Also, a hydrophilic substrate can trap (or attract) water molecules (from Langmuir trough), which with time evaporate to form drying-mediated agglomeration and nanopatterning of DT-AuNPs.²³ Similarly, a hydrophobic substrate, due to its repulsive nature on water (for LB deposition),

Saha Institute of Nuclear Physics, 1/AF Bidhannagar, Kolkata 700064, India.

E-mail: satyajit.hazra@saha.ac.in

† Electronic supplementary information (ESI) available. See DOI: 10.1039/c7cp07236h

‡ Current address: B. R. A. Bihar University, Muzaffarpur 842001, India.

can perturb and change the monolayer structure, which with time can reorganize to release the strain. On the other hand, the hydrophobic substrate, due to its attractive nature on the DT-AuNP Langmuir monolayer (during LS deposition), is expected to create the least disturbance.¹² Although this is presumably the better choice for the formation of uniform nanostructures over large areas on solid substrates just by tuning the DT-AuNP monolayer structures at the air/water interface, the question is, in practice, is it really possible? To address this question it is important to know if the hydrophobic strength of the substrate matters at all in creating the least disturbance on the DT-AuNP Langmuir monolayer or not. Also, it is necessary to know if the ambient conditions create any instability in the transferred film to change the structure with time or not.

It is known that the hydrophobic strength of the substrate can be tuned through termination or passivation of the substrate, differently, which essentially modifies the surface free energy or contact angle.^{28–33} Though different terminated substrates were used for the growth of DT-AuNP LS films, the carbon-coated grids were mostly used as hydrophobic substrates to study the structures of the Langmuir monolayers, indirectly, using transmission electron microscopy (TEM).³⁴ DT-AuNP LS films were also grown on other large hydrophobic substrates, namely H-passivated Si substrates, to study the structure of the films, using X-ray scattering techniques;¹² however, no systematic work was carried out to compare the structures of the DT-AuNP LS films grown on different hydrophobic (strength) substrates. On the other hand, the ambient conditions can change the passivation of the substrate with time, even in the presence of a film, which in turn can influence the structure of the film. For example, an oxide layer was found to grow on Si substrates by replacing the passivated H, Br or Cl atoms, in the presence of metal (Au, Ag), metal–organic (NiA LB) or organic–inorganic (CTAB–silica) nanolayer films to change the film-structures.^{29–33} Also, the ambient conditions can directly change the structure of the film, through oxidation (due to ambient oxygen), interdiffusion (due to ambient pressure), fluctuation, diffusion or reorganization (due to room temperature thermal energy or solvent evaporation), *etc.* For example, oxidation of metals (such as Fe, Cu, Ni, *etc.*) is very common, while interdiffusion of Au inside H-Si substrates and reorganization of DT-AuNPs on O-Si substrates have been reported,^{23,35} all of which lead to a change in the film-structure with time under ambient conditions. However, no attempt was made to find out and compare the structural stability/instability of the DT-AuNP LS films on different hydrophobic substrates under ambient conditions.

Here, the effects of the hydrophobic strength of the substrate and ambient conditions on the structures and stability of DT-AuNP LS films have been investigated, using the X-ray reflectivity (XR) technique,^{36,37} to understand the possibility of the formation of uniform nanostructures over large areas on solid substrates just by tuning the DT-AuNP Langmuir monolayer structures. Different initial structures (monolayer or monolayer plus bilayer) are observed for films deposited on different passivated Si substrates, which indeed suggests a strong role of hydrophobic strength in mimicking the Langmuir

monolayer structure. Structural evolution of the film is observed with time, which is actually a hindrance in the formation of desired nanostructures of DT-AuNPs on solid substrates just by tuning the DT-AuNP monolayer structures at the air/water interface but formation of a similar expanded monolayer structure of DT-AuNPs is observed through evolution, which is interesting. The probable reasons behind these different observations are discussed.

2 Experimental section

2.1 Preparation of DT-AuNP LS films

The synthesis details of DT-AuNPs were reported before.¹² In short, colloidal AuNPs were synthesized following a two-phase (water–toluene) reduction of hydrogen tetrachloroaurate by sodium borohydride in the presence of dodecanethiol³⁸ and the mean diameter of the particles is controlled by tuning the Au : thiol molar ratio,³⁹ which in this case is about 2.5 nm.¹²

Langmuir monolayers of DT-AuNPs were formed in a Langmuir trough (KSV 5000) as reported before.¹² In brief, DT-AuNPs dissolved in toluene solution were spread uniformly on the water surface and were kept undisturbed for some time to let the toluene evaporate and the hydrophobic DT-AuNPs lay suspended at the air–water interface (at 23 °C). The pressure (Π) of the DT-AuNP Langmuir monolayer was regulated by the barrier movement. Prior to the DT-AuNP monolayer deposition, Si substrates (of size about 15 × 15 mm²) were first sonicated in acetone and ethanol solvents to remove organic contaminants and then one set of Si substrates was treated with hydrogen fluoride [HF, Merck, 10%] solution to prepare H-terminated Si (H-Si) substrates,^{12,28} while the other set of Si substrates was immersed in trichloro(octadecyl)silane [OTS, CH₃(CH₂)₁₇SiCl₃] solution to prepare OTS (of monolayer thickness) self-assembled Si (OTS-Si) substrates.⁴⁰ The DT-AuNP Langmuir monolayers formed at different pressures (namely $\Pi = 2, 4, 6$ and 10 mN m⁻¹) of pressure–area (Π - A) isotherm (Fig. S1 of ESI[†]) were then transferred once onto both OTS-Si and H-Si substrates using the LS deposition technique,^{12,41} and are labeled as DT-AuNP/OTS-Si and DT-AuNP/H-Si, respectively. The approach speed, contact duration and removal speed used for the transfer process were 1 mm min⁻¹, 15 s and 1 mm min⁻¹, respectively. The samples were then preserved at the X-ray laboratory, where the temperature and relative humidity were maintained at ~25 °C and ~40%, respectively.

2.2 Characterization of the DT-AuNP LS films

The details of the evolution of the films with time were characterized using XR techniques, while after evolution they were characterized using the AFM technique. The XR measurements of the films were performed using a versatile X-ray diffractometer (VXRD) setup,^{12,42} to get statistically averaged electron density information. VXRD consists of a diffractometer (D8 Discover, Bruker AXS) with a Cu source (sealed tube) followed by a Göbel mirror to select and enhance Cu K α radiation ($\lambda = 1.54$ Å) and further followed by slits to define the size

(0.2 mm × 10 mm) of the beam. The diffractometer has a two-circle goniometer [$\theta(\omega) - 2\theta$] with a quarter-circle Eulerian cradle as a sample stage. The latter has two circular (χ and ϕ) and three translational (X , Y , and Z) motions. The scattered beam was detected using a NaI scintillation (point) detector. Data were taken in the specular condition, *i.e.* the reflected angle is equal to the incident angle, θ . Under such conditions there exists a non-vanishing wave vector component, q_z , which is equal to $(4\pi/\lambda)\sin\theta$ with resolution 0.002 \AA^{-1} . XR data essentially provides an electron-density profile (EDP), *i.e.*, in-plane (x - y) average electron density (ρ) as a function of depth (z) in high resolution.³⁰ From EDP it is possible to estimate not only the film thickness, electron density, and interfacial roughness but also the vertical position of the DT-AuNPs in the film and their evolution with time.

The detailed top surface morphology of the films was mapped using the AFM (5500 AFM, Agilent) technique,^{12,43} a few days after deposition, *i.e.* after evolution under ambient conditions. Topographic images were collected in a noncontact (or intermittent contact) mode to minimize the silicon-tip-induced damage of the soft film. Scans of different sizes and in different portions of the sample were carried out to get statistically meaningful information about the topography.

3 Results and discussion

3.1 Atomic force microscopy and topography

Typical AFM images of the DT-AuNP/OTS-Si LS films obtained after evolution at ambient conditions are presented in Fig. 1. The network-like structures of the films with voids are clearly evident from these images. The network-like structures are predominantly of monolayer height with some fraction having

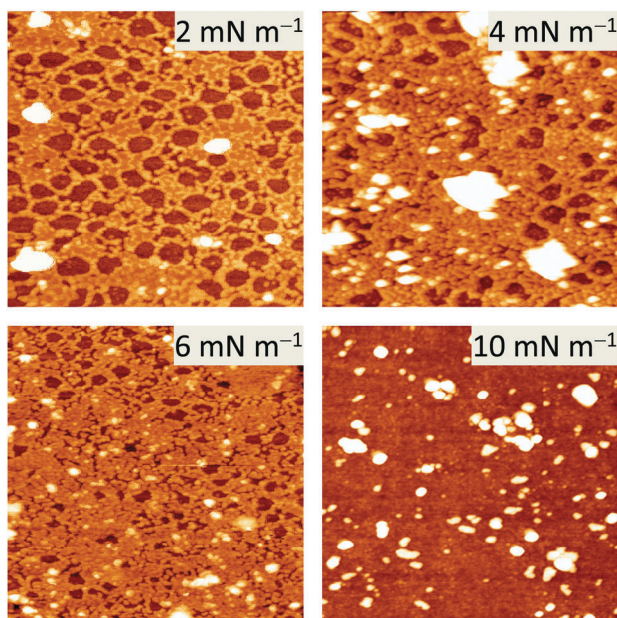


Fig. 1 AFM images (scan size = $2 \times 2 \mu\text{m}^2$) of the time evolved DT-AuNP/OTS-Si LS films deposited at different surface pressures (Π). Dark and light colors represent low and high heights, respectively.

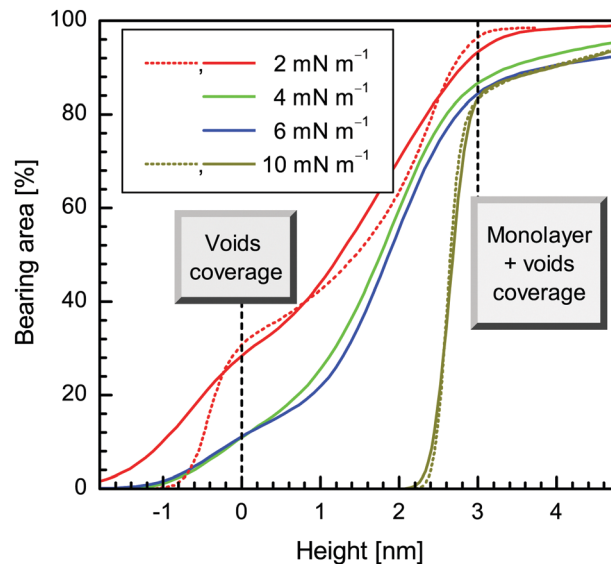


Fig. 2 Bearing area as a function of height (as obtained from AFM images) of the time evolved DT-AuNP/OTS-Si LS films deposited at different surface pressures (Π) showing the void coverage and monolayer (including voids) coverage, as indicated.

a height more than that (indicated by bright white color). The size of the voids is quite large in the film deposited at low Π -value (2 mN m^{-1}) and almost negligible in the film deposited at high Π -value (10 mN m^{-1}). The information about the coverage of the voids and the materials (of different heights) in the films is better obtained from the bearing plots^{44,45} of the AFM images as shown in Fig. 2. It is found that for the film deposited at $\Pi = 2 \text{ mN m}^{-1}$, the coverage of voids is $>30\%$ and that of a film of monolayer height ($\sim 3 \text{ nm}$) is $<70\%$. For the films deposited at $\Pi = 4$ and 6 mN m^{-1} , the coverage of voids is $\sim 10\%$ and that of the film is $\sim 90\%$ of which $\sim 75\%$ is of monolayer height. Finally for the film deposited at $\Pi = 10 \text{ mN m}^{-1}$, the coverage of voids is $\sim 0\%$ and that of the film is $\sim 100\%$ of which $\sim 85\%$ is of monolayer height.

The topography of the DT-AuNP/H-Si LS films obtained after evolution at ambient conditions were presented before,¹² where a 2D-network of disk-like islands of monolayer height on H-Si substrates was very much evident. The size of such islands is found to increase with pressure more systematically on H-Si substrates compared to that on OTS-Si substrates. More voids are found in the DT-AuNP/H-Si LS films obtained from the bearing plots (Fig. S2 of ESI[†]) compared to the DT-AuNP/OTS-Si LS films. The difference is especially appreciable for the films deposited at high Π -value. Also the heights of the monolayer with respect to the voids in the DT-AuNP/H-Si LS films (Fig. S2 of ESI[†]) are found to be lower compared to the DT-AuNP/OTS-Si LS films. The difference is prominent for the DT-AuNP/H-Si LS film deposited at low Π -value.

3.2 X-ray reflectivity and electron density profile

Time evolution XR data of DT-AuNP/OTS-Si and DT-AuNP/H-Si LS films deposited at different Π -values are shown in Fig. 3 and 4. Oscillations with slightly different periodicity and amplitude

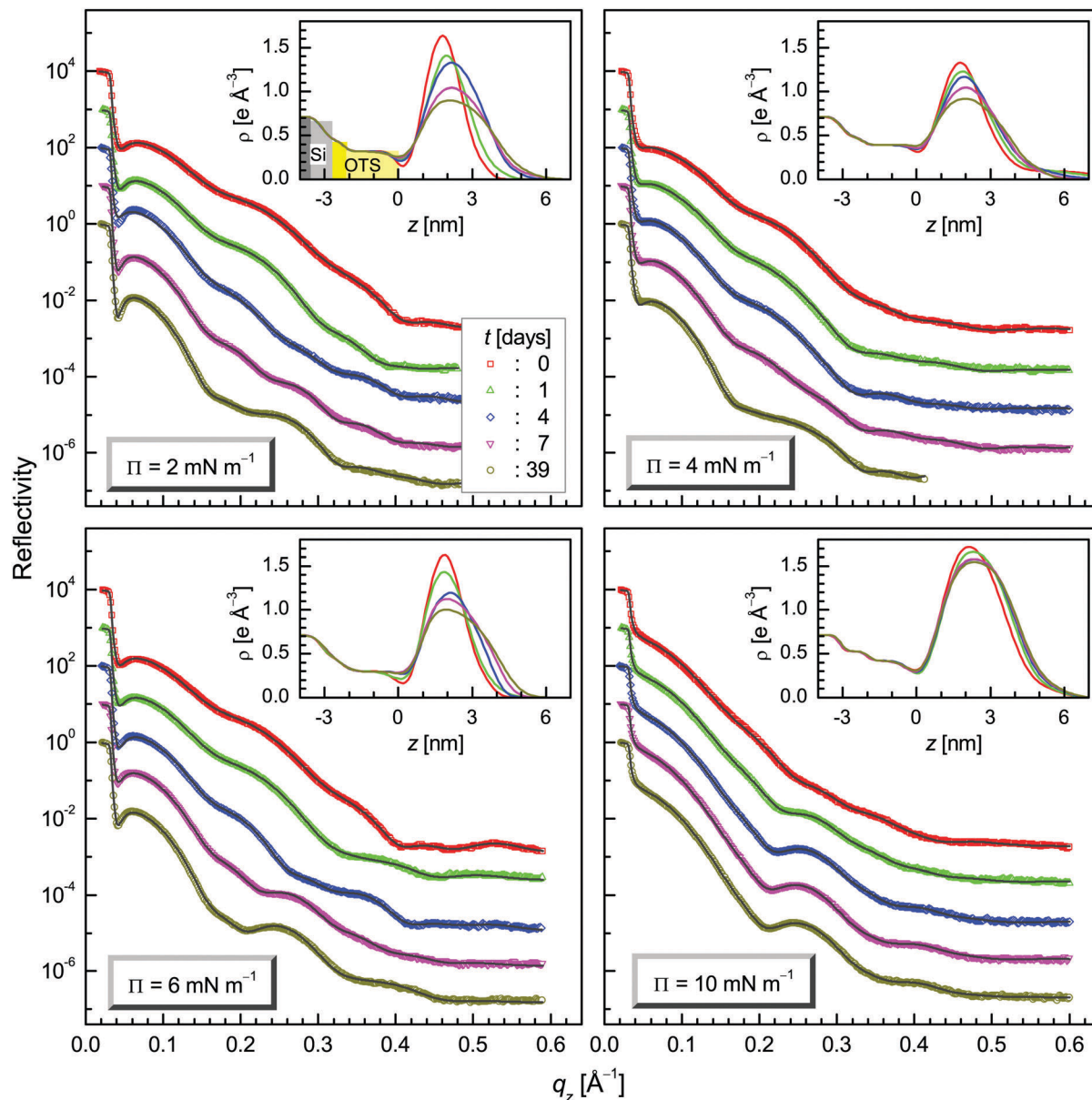


Fig. 3 Time evolution XRD data (different symbols) and analyzed curves (solid lines) of the DT-AuNP/OTS-Si LS films deposited at different surface pressures (Π). Curves are shifted vertically for clarity. Insets: Corresponding analyzed electron density profiles.

are observed in the XRD profiles of the as-deposited DT-AuNP/OTS-Si LS films (Fig. 3). Such periodicity changes with time suggest change in the film structure. The change is, however, minimum for the film deposited at high pressure ($\Pi = 10 \text{ mN m}^{-1}$). A broad peak or hump followed by a dip is mainly observed in the XRD profiles of DT-AuNP/H-Si LS films (Fig. 4). The sharpness of the hump and the position of the dip (as indicated by the dashed line) are found to decrease with time. However, the decrease in the position is prominent for the low Π -value film and almost negligible for the high Π -value film suggesting large thickness change for the previous one, while small thickness change for the latter.

To get quantitative information about the films, all XRD profiles were analyzed using Parratt's formalism,⁴⁶ after incorporating

roughness at each interface.³⁰ An instrumental resolution in the form of a Gaussian function and a constant background were also included at the time of data analysis. It can be noted that the off-specular reflectivity and diffuse scattering profiles for the films were checked and it was found that the diffuse contribution is much less compared to the specular one and thus its contribution was neglected for further XRD (specular) data analysis. For the analysis of the XRD profiles of DT-AuNP/OTS-Si LS films, first a monolayer of DT-AuNPs of different thickness and coverage on the OTS-Si substrate was considered. Next each DT-AuNP monolayer was further considered to be made of three layers, namely a thiol-rich low density bottom layer, an Au-rich high density middle layer and again a thiol-rich low density top layer. Also, the OTS-Si substrate was considered to be made of

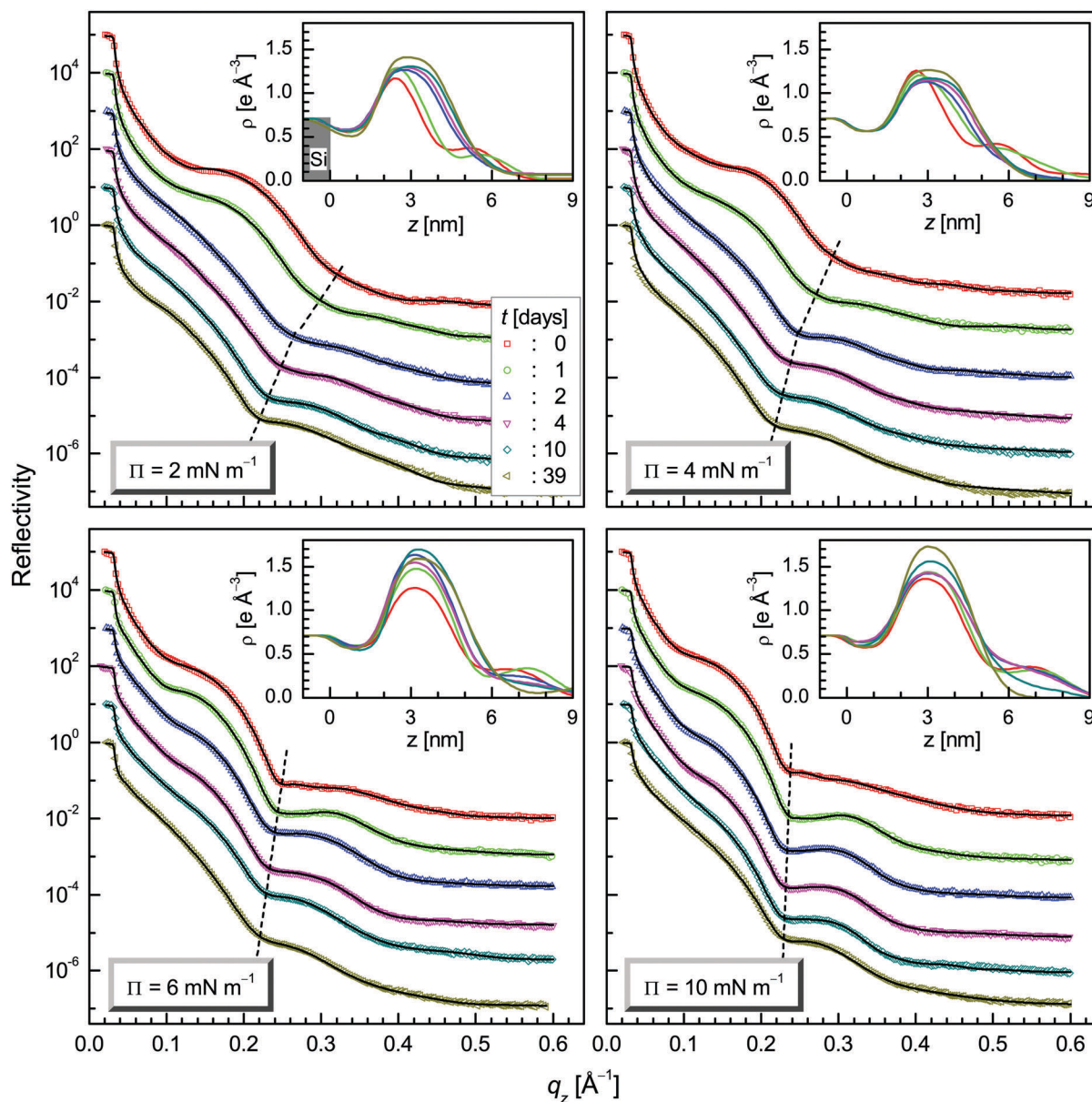


Fig. 4 Time evolution XRD data (different symbols) and analyzed curves (solid lines) of the DT-AuNP/H-Si LS films deposited at different surface pressures (Π). Curves are shifted vertically for clarity. Insets: Corresponding analyzed electron density profiles.

three layers, namely a high density Si substrate at the bottom, an intermediate density silane related layer at the middle and a low density hydrocarbon layer on the top. The starting EDPs of the OTS-Si substrates were used considering ideal SAM structure and then some allowance was given to the top two layers to find out the actual EDPs of the OTS-Si substrates for each film from the initially measured XRD data. For the analysis of the XRD data, measured at the subsequent stages, the initial EDP of the OTS-Si substrate was kept fixed apart from the top roughness. The parameters corresponding to the DT-AuNP monolayer were, however, varied to fit the XRD profiles. The best fit XRD profiles along with the corresponding EDPs for all the films are shown in Fig. 3. Similarly, the XRD profiles of DT-AuNP/H-Si LS films were analyzed considering a monolayer of DT-AuNPs of different

thickness and coverage on the H-Si substrate first and subsequently a second layer of low coverage was added, if required. Each DT-AuNP layer was again considered to be made of three layers, as before. The best fitted XRD profiles along with the corresponding EDPs, thus obtained for all the films are shown in Fig. 4.

Two peaks (one intense and another weak) are clearly visible (see Fig. 4) in the EDPs of the DT-AuNP/H-Si LS films at the initial stages. With time such distinct nature disappears and a rather broad single peak appears. On the other hand, a single peak is only observed (Fig. 3) in the EDPs of the DT-AuNP/OTS-Si LS films at all stages. However, the EDPs for both the systems are found to change with Π -value and time. The change is mainly related to the peak or maximum value (ρ_m) and the full width at

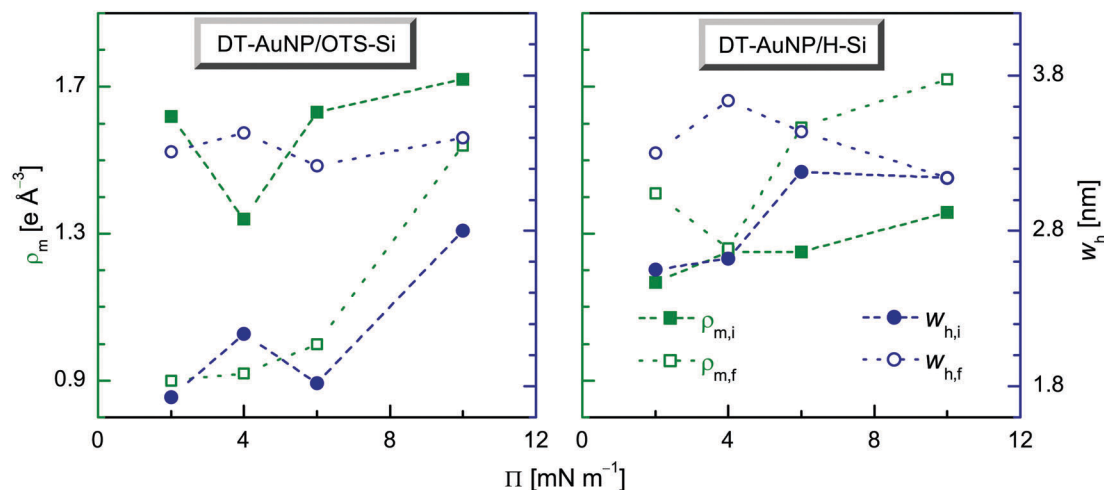


Fig. 5 Variation of initial and final peak electron density ($\rho_{m,i}$ and $\rho_{m,f}$) and peak width ($w_{h,i}$ and $w_{h,f}$) of the films with deposited surface pressure (Π) for the DT-AuNP/OTS-Si and DT-AuNP/H-Si LS systems.

Table 1 Parameters such as the peak electron density ($\rho_{m,i}$ and $\rho_{m,f}$), the full width at half maximum of EDP ($w_{h,i}$ and $w_{h,f}$) and the summation of the deconvoluted Gaussian peak electron densities [$(\sum \rho_{0j})_i$ and $(\sum \rho_{0j})_f$] at initial and final stages ($t \approx 0$ and 39 days) of measurements and the peak-decay or width-growth time (τ) for the DT-AuNP/OTS-Si and/or DT-AuNP/H-Si LS films deposited at different surface pressures (Π)

Π (mN m ⁻¹)	DT-AuNP/OTS-Si					DT-AuNP/H-Si						
	$\rho_{m,i}$ (e Å ⁻³)	$\rho_{m,f}$ (e Å ⁻³)	$w_{h,i}$ (nm)	$w_{h,f}$ (nm)	τ (days)	$\sum \rho_{0j}$ (e Å ⁻³)	$\rho_{m,i}$ (e Å ⁻³)	$\rho_{m,f}$ (e Å ⁻³)	$w_{h,i}$ (nm)	$w_{h,f}$ (nm)	$(\sum \rho_{0j})_i$ (e Å ⁻³)	$(\sum \rho_{0j})_f$ (e Å ⁻³)
2	1.62	0.90	1.73	3.31	4.8	1.63	1.17	1.41	2.55	3.30	1.91	2.61
4	1.34	0.92	2.14	3.43	6.0	1.68	1.25	1.26	2.62	3.64	2.18	2.44
6	1.63	1.00	1.82	3.22	4.2	1.70	1.25	1.59	3.18	3.44	2.46	3.00
10	1.72	1.54	2.80	3.40	2.5	2.75	1.36	1.72	3.14	3.14	2.74	2.96

half maximum (w_h) of the EDP. The variation of these two parameters at initial (i) and final (f) stages of measurements are plotted as a function of Π -value in Fig. 5 for both the systems, separately and also tabulated in Table 1. It can be observed that for the DT-AuNP/OTS-Si LS system, the $\rho_{m,i}$ -value remains almost the same (~ 1.6 e Å⁻³) for $\Pi = 2$ and 6 mN m⁻¹, but decreases (to ~ 1.3 e Å⁻³) for $\Pi = 4$ mN m⁻¹ and increases (to ~ 1.7 e Å⁻³) for $\Pi = 10$ mN m⁻¹. Similarly, the $w_{h,i}$ -value remains almost the same (~ 1.7 nm) for $\Pi = 2$ and 6 mN m⁻¹, but increases reasonably (to ~ 2.2 nm) for $\Pi = 4$ mN m⁻¹ and appreciably (to ~ 2.8 nm) for $\Pi = 10$ mN m⁻¹. This means that both the parameters either remain unchanged or increase with Π -value with some deviation at $\Pi = 4$ mN m⁻¹ and the amount of material in the films (obtained from the combination of both the parameters) increases very little upto $\Pi = 6$ mN m⁻¹ and appreciably thereafter. On the other hand, the $\rho_{m,f}$ -value is found to increase gradually (from 0.9 to 1.5 e Å⁻³) with the increase in Π -value. The increase is very small upto $\Pi = 6$ mN m⁻¹ and appreciable after that. While the $w_{h,f}$ -value is found to be quite high (~ 3.4 nm) and almost similar for all the Π -values. For the DT-AuNP/H-Si LS system, the value of $\rho_{m,i}$ is found to increase from 1.2 to 1.4 e Å⁻³ with the increase of Π -value. Similarly, the value of $w_{h,i}$ (estimated from the width of the intense peak) is found to increase from 2.6 to 3.2 nm with the increase of Π -value. The amount of material in the films show a small gradual increase with Π -value. On the other hand, the $\rho_{m,f}$ -value

is found to increase (from 1.2 to 1.7 e Å⁻³) and the $w_{h,f}$ -value is found to decrease (~ 3.6 to 3.1 nm) with the increase of Π -value with some deviation at low Π -value.

3.3 Electron density profile: time-dependence

In order to understand the time-dependent nature of the films, the variations of ρ_m and w_h with time (as obtained from Fig. 3 and 4) are shown in Fig. 6 and 7 for the DT-AuNP/OTS-Si and DT-AuNP/H-Si LS films deposited at different Π values. The variations are found to be systematic only for the DT-AuNP/OTS-Si LS films, where the value of ρ_m (or w_h) initially decreases (or increases) and then saturates with time. Such variation of ρ_m and w_h with time (t) at ambient conditions can be expressed quantitatively using standard exponential dependence:

$$\rho_m(t) = \Delta\rho_m e^{-t/\tau} + \rho_{m\infty} \quad (1)$$

$$w_h(t) = w_{h0} + \Delta w_h (1 - e^{-t/\tau}) \quad (2)$$

where τ in eqn (1) is the decay-time, $\Delta\rho_m = \rho_{m0} - \rho_{m\infty}$ is the maximum change in ρ_m , ρ_{m0} is its maximum value at $t \rightarrow 0$ and $\rho_{m\infty}$ is its minimum or saturation value at $t \rightarrow \infty$, while τ in eqn (2) is the growth-time, $\Delta w_h = w_{h\infty} - w_{h0}$ is the maximum change in w_h , w_{h0} is its minimum value at $t \rightarrow 0$ and $w_{h\infty}$ is its maximum or saturation value at $t \rightarrow \infty$. Considering $\rho_{m0} \approx \rho_{m,i}$, $\rho_{m\infty} \approx \rho_{m,f}$, $w_{h0} \approx w_{h,i}$ and $w_{h\infty} \approx w_{h,f}$, the variations of ρ_m and w_h for the DT-AuNP/OTS-Si LS films have been simulated

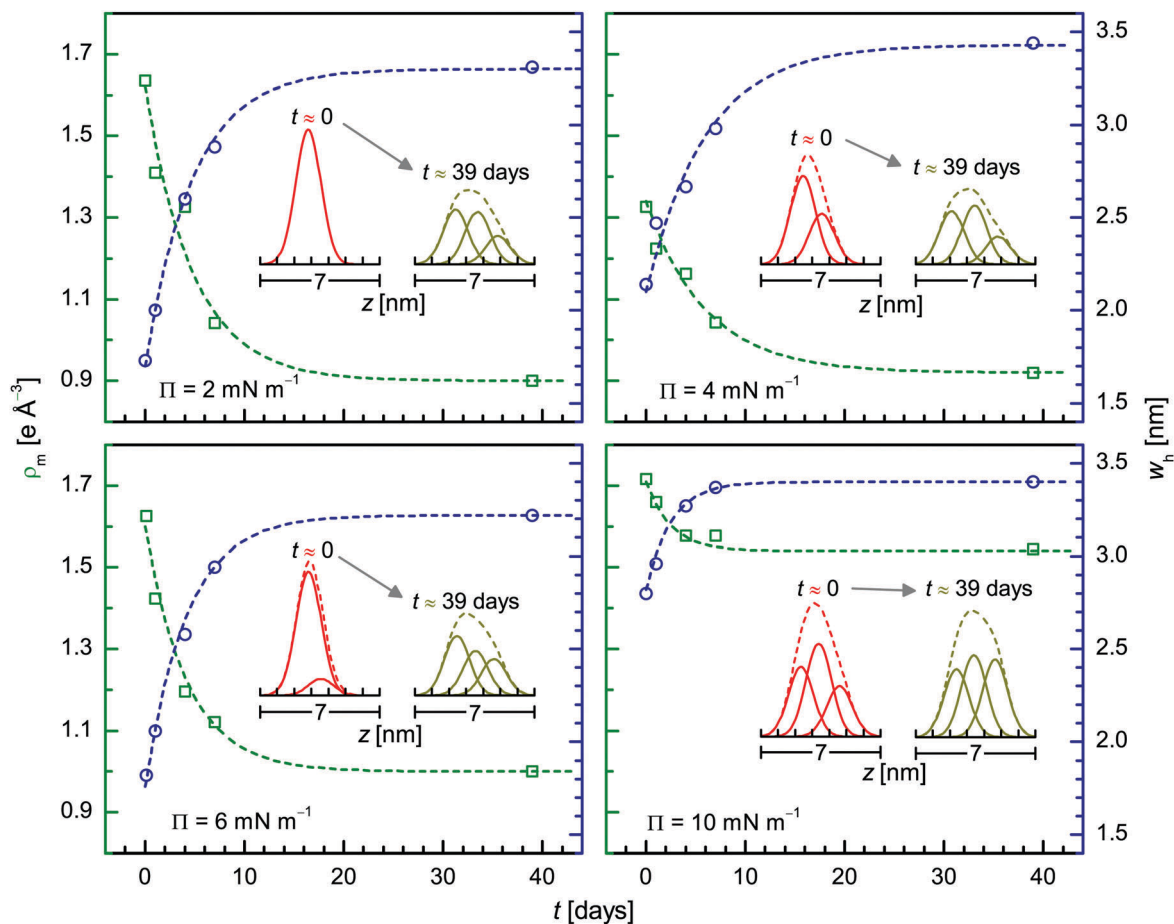


Fig. 6 Evolution of peak electron density (ρ_m) and peak width (w_h) with time of the DT-AuNP/OTS-Si LS films deposited at different surface pressures (Π). Dashed lines through the data are the analyzed curves. Insets: Corresponding initial ($t \approx 0$) and final ($t \approx 39$ days) EDPs and their Gaussian deconvolution to show the vertical organization of DT-AuNPs and their reorganization with time.

using eqn (1) and (2), respectively, and the simulated profiles are shown in Fig. 6. The values of the parameter τ , used for the simulation, are enlisted in Table 1.

In order to model the evolution of the film with time, quantitative reconstructions of EDPs are essential. In general, the depth-dependent electron density can be expressed as:

$$\rho(z) = \rho_s(z) + \rho_F(z) \quad (3)$$

where the first term of the right hand side corresponds to the substrate of uniform electron density with some variation at the top due to surface roughness and the second term corresponds to the film, which is of prime importance. Here the film is composed of DT-AuNPs, where the EDP of a single DT-AuNP can be calculated considering the core-shell structure and can be approximated with a Gaussian peak function, $\rho_0 \exp[-(z/\sigma_0)^2]$, of $\rho_0 \approx 1.8 \text{ e \AA}^{-3}$ and $\sigma_0 \approx 1.04 \text{ nm}$ as shown schematically in Fig. 8. Accordingly, $\rho_F(z)$ can be expressed as the summation of Gaussian peaks:

$$\rho_F(z) = \sum_j \rho_{0j} \exp \left[- \left(\frac{z - z_{0j}}{\sigma_0} \right)^2 \right] \quad (4)$$

where ρ_{0j} is the peak value, z_{0j} is the position and σ_0 is the standard deviation or width related term of the j th Gaussian peak. It can be noted that each Gaussian peak in eqn (4) arises from a layer consisting of DT-AuNPs and not simply from a single DT-AuNP. Accordingly, $\sigma_0 \approx 1.04 \text{ nm}$ in eqn (4) corresponds to a layer of perfect monolayer thickness, while ρ_{0j} corresponds to the coverage of DT-AuNPs in the monolayer at z_{0j} . Eqn (4) is then used to simulate the EDPs of the films by considering the minimum possible number of Gaussian peaks. Deconvoluted profiles obtained from the simulation of the EDPs for all the films at initial and final stages are shown in Fig. 6 and 7. The integrated EDP (Int EDP), which is proportional to the summation of the deconvoluted Gaussian peak values, $\sum \rho_{0j}$ (see eqn (S2) and (S3) of ESI†) and correlated to the amount of materials in a film, is expected to be time-independent. Although this is the case for the DT-AuNP/OTS-Si LS films, it is not the case for the DT-AuNP/H-Si LS films (as clearly evident in Fig. S3 and S4 of ESI†). Accordingly, only the initial $\sum \rho_{0j}$ value for the DT-AuNP/OTS-Si LS films and both initial and final $\sum \rho_{0j}$ values for the DT-AuNP/H-Si LS films are presented in Table 1.

It is evident from the value of $\sum \rho_{0j}$ that the DT-AuNP/OTS-Si LS films can be categorized into two groups: low Π -value

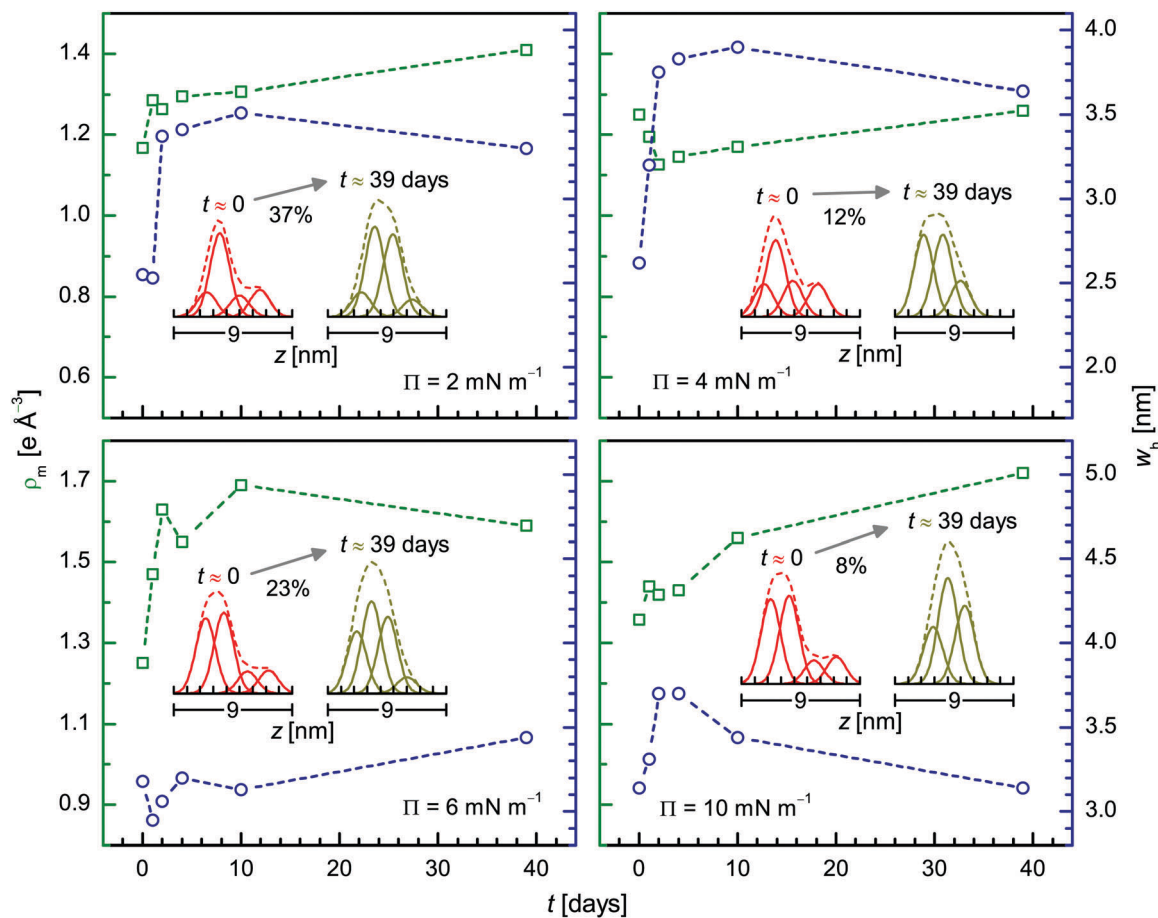


Fig. 7 Evolution of peak electron density (ρ_m) and peak width (w_n) with time of the DT-AuNP/H-Si LS film deposited at different surface pressures (Π). Dashed lines through the data are to guide the eyes. Insets: Corresponding initial ($t \approx 0$) and final ($t \approx 39$ days) EDPs and their Gaussian deconvolution to show the vertical organization of DT-AuNPs and their reorganization with time. The observed apparent percentage increase in the amount of DT-AuNPs with time is indicated.

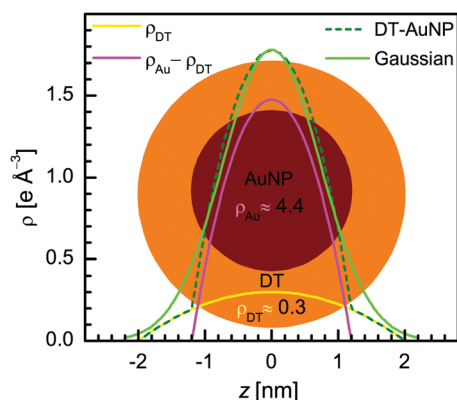


Fig. 8 Schematic of a DT-AuNP, where the core is of high density Au ($\rho_{Au} \approx 4.4 \text{ e } \text{\AA}^{-3}$) and the coating layer is of low density DT ($\rho_{DT} \approx 0.3 \text{ e } \text{\AA}^{-3}$). Corresponding variations of calculated electron density as a function of height (relative to the center of DT-AuNP); for the complete NP of size $\approx 4 \text{ nm}$ and $\rho \approx \rho_{DT}$, for the core NP of size $\approx 2.5 \text{ nm}$ and $\rho \approx \rho_{Au} - \rho_{DT} (\approx 4.1 \text{ e } \text{\AA}^{-3})$, for the linear combination of them and for the equivalent Gaussian function.

(2, 4 and 6 mN m^{-1}) films, where $\sum \rho_{0j} \approx 1.7 \text{ e } \text{\AA}^{-3}$ and high Π -value (10 mN m^{-1}) films, where $\sum \rho_{0j} \approx 2.7 \text{ e } \text{\AA}^{-3}$. These

$\sum \rho_{0j}$ values apparently indicate full monolayer coverage for the first group of films and more than monolayer coverage for the second group of films. However, it is clear from the AFM images (Fig. 1) and the corresponding bearing plots (Fig. 2) that the monolayer coverage is not complete, rather voids are present within network-like structures for the first group of films. The absence of such effect (of voids) in the $\sum \rho_{0j}$ value suggests that the voids do not contribute to the ρ value estimated from the XR analysis. This is possible if the size of the voids is comparable to the coherent length of the X-ray beam. In that case, the covered film area and the void area scattered incoherently⁴⁷ and the scattering from the covered parts only contributes to the overall signal (as clarified in ESI†). The signature of incomplete monolayer coverage is also available from the values of $\Delta \rho_m$ and τ . The large values of both the parameters indicate less restrictive motion of the AuNPs in the film. This can happen if the coverage is incomplete, as the AuNPs close to voids can have less restrictive motions (due to asymmetric in-plane interaction) compared to those within covered areas. On the other hand, the values of $\sum \rho_{0j}$ for the DT-AuNP/H-Si LS films are neither similar to that of the DT-AuNP/OTS-Si LS films nor time-independent. The increase in the value of this parameter

with time is likely due to the growth of a hygroscopic oxide layer on the substrate surface (inside the voids) and increase in the area of the large size voids. The growth of an oxide layer (evident from the low heights of the monolayer with respect to the voids in Fig. S2 of ESI†) is applicable to all the voids, while the incoherent scattering concept is applicable additionally to the very large size voids only, which are mainly present in the films deposited at low Π -values (elaborated in the ESI†).

3.4 Growth and evaluation mechanisms

Now, let us first try to model the structures of the films and then try to understand their growth and evaluation mechanisms. The structures of the DT-AuNP LS films grown at low and high pressures (*i.e.* $\Pi = 2$ and 10 mN m^{-1}) on two different passivated substrates (OTS-Si and H-Si) at initial and final stages (*i.e.* $t \approx 0$ and 39 days), as visualized from the analysis, are shown schematically in Fig. 9. Accordingly, the DT-AuNP/OTS-Si LS film deposited at low pressure consists of a monolayer structure with large size voids (*i.e.* partial coverage), where initially (Fig. 9a) all the DT-AuNPs are at the same z position to give rise to a layer of perfect monolayer thickness and finally (Fig. 9b) a few of them are at slightly different z positions to give rise to a fluctuating monolayer (of thickness intermediate between monolayer and bilayer thickness). The DT-AuNP/H-Si LS film deposited at low pressure initially (Fig. 9c) consists of monolayer plus a very small fraction of bilayer structures with large size voids (*i.e.* partial coverage), which with time finally (Fig. 9d) becomes a symmetrically fluctuated monolayer structure (of thickness intermediate between monolayer and bilayer thickness) with increased void size. The DT-AuNP/OTS-Si LS film deposited at high pressure consists of a highly fluctuated monolayer structure with negligible voids (*i.e.* full coverage), where most of the DT-AuNPs are initially (Fig. 9e) placed at the central position and finally (Fig. 9f) distributed evenly to give rise to a thickness less than bilayer thickness. Finally, the DT-AuNP/H-Si LS film deposited at high pressure initially (Fig. 9g) consists

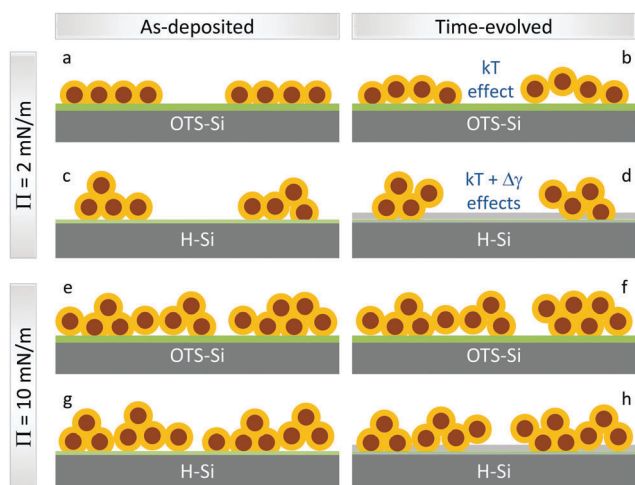


Fig. 9 Structural models of the as-deposited ($t \approx 0$) and time-evolved ($t \approx 39$ days) DT-AuNP LS films deposited at low and high surface pressures (Π) on the OTS-Si and H-Si substrates.

of monolayer plus small bilayer structures with negligible voids (*i.e.* full coverage), which with time finally (Fig. 9h) becomes a more symmetrically fluctuated monolayer structure (of thickness intermediate between monolayer and bilayer thickness) with some voids.

It is known that the DT-AuNPs on the water surface first self-assembled around different points to form disk-like islands of monolayer height¹² (due to the complex balance of long range vdW attractions and short range steric repulsion of the DT-AuNPs^{13–18} initiated by solvent evaporation^{19–21} in the presence of the hydrophobic repulsion of water), which on compression formed a 2D-network of buckled or flipped disk-like islands^{12,48} (due to a combined effect of collision induced coalescence and solid-like behavior resisting deformation of the islands¹³). The interactions between DT-AuNPs in the islands can be described phenomenologically by a potential given by Hamaker.^{49–52} Considering the size ($2R \approx 2.5 \text{ nm}$, as estimated from the optical absorption and TEM measurements), the centre-to-centre separation ($D \approx 4 \text{ nm}$, as estimated from the GISAXS measurements for the DT-AuNP/H-Si LS films)¹² *i.e.* the edge-to-edge separation ($\delta = D - 2R \approx 1.5 \text{ nm}$) and the Hamaker constant ($A \approx 1.95 \text{ eV}$)^{50,51} of the AuNPs, the interaction potential energy is less than 10 meV . The growth and evaluation of such Langmuir monolayers when transferred onto OTS-Si and H-Si substrates using LS techniques can be understood from the XR data analyses, which are shown schematically in Fig. 10. During LS deposition (Fig. 10a and b), the hydrophobic DT-AuNPs in the Langmuir monolayer feel repulsion from the hydrophilic water and attraction from the hydrophobic substrate.

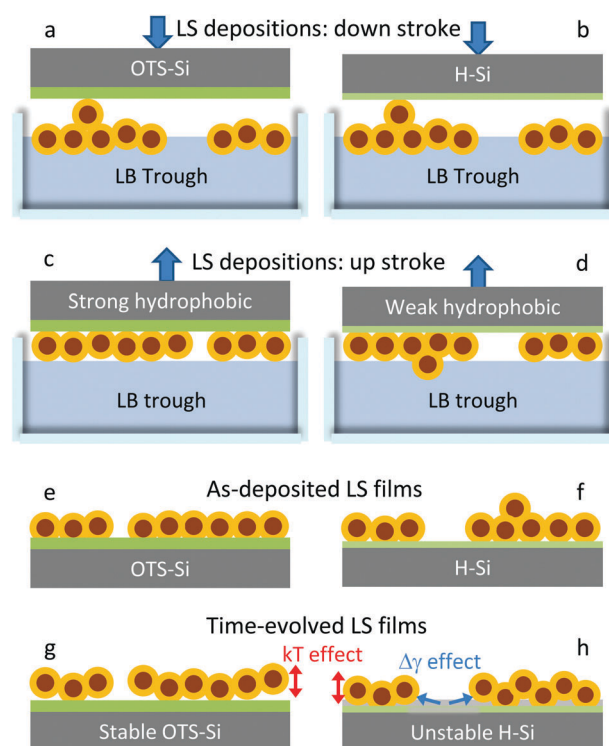


Fig. 10 Schematic illustration of the growth and evolution of DT-AuNP LS films on OTS-Si and H-Si substrates.

The relatively strong-hydrophobic OTS-Si substrate (contact angle $\theta_c \approx 110^\circ$),^{40,53} however, creates strong-attraction towards DT-AuNPs (Fig. 10c) to form (Fig. 10e) a partially covered monolayer structure (with perfect monolayer thickness) at low pressure (Fig. 9a) and a nearly covered buckled monolayer structure (with enhanced monolayer thickness) at high pressure (Fig. 9e). The weak-hydrophobic H-Si substrate ($\theta_c \approx 80^\circ$),⁵⁴ on the other hand, creates relatively weak-attraction towards DT-AuNPs (Fig. 10d) to form (Fig. 10f) a partially covered monolayer structure (containing very small fraction of bilayer) at low pressure (Fig. 9c) and a nearly covered monolayer structure (containing small fraction of bilayer) at high pressure (Fig. 9g).

After deposition, evolution of the film takes place with time (Fig. 10g and h). Such evolution is unlikely to be drying mediated,²³ as no trapped water is expected on the hydrophobic particles and/or substrates. Also, the evolution is unlikely to relax the strain, which may usually arise due to the hydrophobic substrate–water repulsion (for LB deposition) or the substrate–film repulsion (for hydrophilic substrate) during deposition, as such strain is not expected for the LS deposition on hydrophobic substrates. It is expected that at ambient conditions, the room temperature (T) supplies thermal energy $kT \approx 26$ meV (where k is the Boltzmann constant) to the system, which can change the positions of the DT-AuNPs. The amount and direction of the change, are however, dependent upon their interactions in the film. The absence of water or repulsive force on the top of the film (which was present during deposition) probably allows the small thermal energy to fluctuate and migrate the DT-AuNPs along the accessible out-of-plane direction to change the film-thickness with time. Such kT effect is applicable to the films deposited on both the substrates (Fig. 10g and h). Additionally, instability of the passivated Si surface, at ambient conditions, plays an important role. It is known that the OTS-Si substrate is stable^{40,53} but the H-Si substrate is not.^{29–32} For the latter, desorption of H atoms followed by the growth of an oxide layer takes place with time, which then changes its surface energy or hydrophobic/hydrophilic nature from weak-hydrophobic ($\theta_c \approx 80^\circ$ for H-Si) to weak-hydrophilic ($\theta_c \approx 60^\circ$ for O-Si) or moderate-hydrophilic ($\theta_c \approx 20^\circ$ for OH-Si).^{33,54,55} Such change in the hydrophobic/hydrophilic nature (*i.e.* contact angle $\Delta\theta_c$) or the substrate surface energy ($\Delta\gamma$, which is related to $\Delta\theta_c$) can even take place in the presence of a film, through voids, which essentially changes the film–substrate interaction. This $\Delta\gamma$ effect will be appreciable in the void portion of the films deposited on H-Si substrates, and accordingly, the DT-AuNPs near the periphery of the voids will experience inward force to enhance the size of the voids (Fig. 10h).

The DT-AuNPs in the Langmuir monolayer, *i.e.* at the air/water interface, do not experience any attraction with the water, but rather feel repulsion. Thus vertical fluctuations and/or flipping of DT-AuNPs at the air/water interface is well expected after solvent evaporation due to the presence of room temperature thermal energy. The strong attraction induced by the OTS-Si substrate, during transfer, is likely to contract the vertical structure through some reorganization and thiol interdigitization into the OTS layer. While the weak attraction

induced by the H-Si substrate is likely to retain or less disturb the vertical structure. Accordingly, a better mimic of a Langmuir monolayer structure is expected on the H-Si substrate compared to the OTS-Si substrate at the initial stages, the trend of which is also evident from the present structural (out-of-plane thickness and in-plane island size) analysis. Subsequently, the spherically symmetric DT-AuNPs, within the film, evolve or fluctuate with time at ambient conditions due to the presence of room temperature thermal energy and/or change in the substrate surface energy (unlike spherically asymmetric amphiphilic molecules, where a perfect 2D structure is more favorable), to form an extended/broad monolayer or compressed/narrow bilayer structure of thickness ≈ 6 nm. The kT effect probably fluctuates the DT-AuNPs mainly along the vertical direction as observed for the films deposited on the OTS-Si substrates, where the film-thickness changes with time following the exponential growth law. The critical growth time (τ) and the change in the film-thickness are prominent for the film deposited at low pressure, where initial film-coverage and film-thickness are low. The combination of kT and $\Delta\gamma$ effects probably fluctuates the DT-AuNPs in different directions as observed for the films deposited on the H-Si substrates. The final thickness, which is more related to the vertical fluctuation, is probably decided by the room temperature thermal energy. However, proper theoretical modeling is needed to support such optimized thickness. Also, further experimental studies are required to find out the uniqueness of such thickness, which are in progress.

4 Conclusions

The effects of hydrophobic strength of the substrate and ambient conditions on the structures and stability of DT-AuNP LS films were investigated using the XR technique for the formation of controlled 2D-structures on solid substrates by mimicking the Langmuir monolayer structures through a single transfer process. A partially covered monolayer structured (with perfect monolayer thickness) film at low pressure and nearly covered buckled monolayer structured (with enhanced monolayer thickness) film at high pressure are evident on the OTS-Si substrate, while a partially covered monolayer plus few bilayer structured film at low pressure and nearly covered monolayer plus few bilayer structured film at high pressure are evident on the H-Si substrate at the initial stages. These indicate that during transfer, the OTS-Si substrate, due to its strong-hydrophobic nature ($\theta_c \approx 110^\circ$), creates too much attraction towards the DT-AuNP Langmuir monolayer to vertically squeeze the structure, while the H-Si substrate, due to its weak-hydrophobic nature ($\theta_c \approx 80^\circ$), creates reasonable attraction towards the DT-AuNP Langmuir monolayer to better mimic the structure. At ambient conditions, all films evolved with time to change the initial film-thickness. The evolution of film-thickness deposited on OTS-Si substrates shows exponential growth due to kT (≈ 26 meV) energy induced systematic diffusion, while those deposited on H-Si substrates show anomalous evolution due to both kT and $\Delta\gamma$ (related to $\Delta\theta \approx 20^\circ$) energy driven

fluctuation. Finally, all the films formed nearly similar vertically expanded monolayer structures, though the evolution paths are different, which is quite interesting and requires further investigation.

Conflicts of interest

There are no conflicts to declare.

References

- C. P. Collier, R. J. Saykally, J. J. Shiang, S. E. Henrichs and J. R. Health, *Science*, 1997, **277**, 1978–1981.
- C. B. Murray, C. R. Kagan and M. G. Bawendi, *Annu. Rev. Mater. Sci.*, 2000, **30**, 545–610.
- Z. Tang, N. A. Kotov and M. Giersig, *Science*, 2002, **297**, 237–240.
- Clusters and Colloids: From Theory to Applications*, ed. G. Schmid, John Wiley & Sons, 2008.
- S. Srivastava, D. Nykypanchuk, M. Fukuto and O. Gang, *ACS Nano*, 2014, **8**, 9857–9866.
- J. Yang, M. K. Choi, D.-H. Kim and T. Hyeon, *Adv. Mater.*, 2016, **28**, 1176–1207.
- Z. Nie, A. Petukhova and E. Kumacheva, *Nat. Nanotechnol.*, 2010, **5**, 15–25.
- Y. Min, M. Akbulut, K. Kristiansen, Y. Golan and J. Israelachvili, *Nat. Mater.*, 2008, **7**, 527–538.
- M. C. Daniel and D. Astruc, *Chem. Rev.*, 2004, **104**, 293–346.
- S. Liu, R. Maoz and J. Sagiv, *Nano Lett.*, 2004, **4**, 845–851.
- M. A. Mezour, I. I. Perepichka, J. Zhu, R. B. Lennox and D. F. Perepichka, *ACS Nano*, 2014, **8**, 2214–2222.
- M. Mukhopadhyay and S. Hazra, *RSC Adv.*, 2016, **6**, 12326–12336.
- V. Santhanam, J. Liu, R. Agarwal and R. P. Andres, *Langmuir*, 2003, **19**, 7881–7887.
- B. Kim, M. A. Carignano, S. L. Tripp and A. Wei, *Langmuir*, 2004, **20**, 9360–9365.
- M. Fukuto, R. K. Heilmann, P. S. Pershan, A. Badia and R. B. Lennox, *J. Chem. Phys.*, 2004, **120**, 3446–3459.
- S. J. Khan, F. Pierce, C. M. Sorensen and A. Chakrabarti, *Langmuir*, 2009, **25**, 13861–13868.
- M. N. Martin, J. I. Basham, P. Chando and S.-K. Eah, *Langmuir*, 2010, **26**, 7410–7417.
- C. P. Joshi, Y. Shim, T. P. Bigioni and J. G. Amar, *Phys. Rev. E: Stat., Nonlinear, Soft Matter Phys.*, 2014, **90**, 032406.
- E. Rabani, D. R. Reichman, P. L. Geissler and L. E. Brus, *Nature*, 2003, **426**, 271–274.
- S. Narayanan, J. Wang and X.-M. Lin, *Phys. Rev. Lett.*, 2004, **93**, 135503.
- T. P. Bigioni, X.-M. Lin, T. T. Nguyen, E. I. Corwin, T. A. Witten and H. M. Jaeger, *Nat. Mater.*, 2006, **5**, 265–270.
- Handbook of Applied Surface and Colloid Chemistry*, ed. K. Holmberg, D. O. Shah and M. J. Schwuger, John Wiley & Sons Ltd., 2002, vol. 1.
- R. Banerjee, S. Hazra, S. Banerjee and M. K. Sanyal, *Phys. Rev. E: Stat., Nonlinear, Soft Matter Phys.*, 2009, **80**, 056204.
- J. F. Galisteo-López, M. Ibisate, R. Sapienza, L. S. Froufe-Pérez, A. Blanco and C. López, *Adv. Mater.*, 2011, **23**, 30–69.
- P. Colson, R. Cloots and C. Henrist, *Langmuir*, 2011, **27**, 12800–12806.
- T. Ishida, Y. Tachikiri, T. Sako, Y. Takahashi and S. Yamada, *Appl. Surf. Sci.*, 2017, **404**, 350–356.
- J. J. Giner-Casares and J. Reguera, *Nanoscale*, 2016, **8**, 16589–16595.
- H. F. Okorn-Schmidt, *IBM J. Res. Dev.*, 1999, **43**, 351–366.
- J. K. Bal and S. Hazra, *Phys. Rev. B: Condens. Matter Mater. Phys.*, 2007, **75**, 205411.
- J. K. Bal and S. Hazra, *Phys. Rev. B: Condens. Matter Mater. Phys.*, 2009, **79**, 155412.
- J. K. Bal, S. Kundu and S. Hazra, *Phys. Rev. B: Condens. Matter Mater. Phys.*, 2010, **81**, 045404.
- P. Chatterjee, S. Hazra and H. Amenitsch, *Soft Matter*, 2012, **8**, 2956–2964.
- P. Chatterjee and S. Hazra, *J. Phys. Chem. C*, 2014, **118**, 11350–11356.
- J. Y. Kim, S. J. Kwon, J.-B. Chang, C. A. Ross, T. A. Hatton and F. Stellacci, *Nano Lett.*, 2016, **16**, 1352–1358.
- J. K. Bal and S. Hazra, *Phys. Rev. B: Condens. Matter Mater. Phys.*, 2009, **79**, 155405.
- I. K. Robinson and D. J. Tweet, *Rep. Prog. Phys.*, 1992, **55**, 599–651.
- X-Ray and Neutron Reflectivity: Principles and Applications*, ed. J. Daillant and A. Gibaud, Springer, Paris, 1999.
- M. Brust, M. Walker, D. Bethell, D. J. Schiffrin and R. Whyman, *J. Chem. Soc., Chem. Commun.*, 1994, 801–802.
- D. V. Leff, P. C. Ohara, J. R. Heath and W. M. Gelbart, *J. Phys. Chem.*, 1995, **99**, 7036–7041.
- S. A. Mirji, *Surf. Interface Anal.*, 2006, **38**, 158–165.
- I. Langmuir and V. J. Schaefer, *J. Am. Chem. Soc.*, 1938, **60**, 1351–1360.
- S. Hazra, *Appl. Surf. Sci.*, 2006, **253**, 2154–2157.
- I. Roy and S. Hazra, *RSC Adv.*, 2017, **7**, 2563–2572.
- S. Kundu, S. Hazra, S. Banerjee, M. K. Sanyal, S. K. Mandal, S. Chaudhuri and A. K. Pal, *J. Phys. D: Appl. Phys.*, 1998, **31**, L73–L77.
- I. Horcas, R. Fernández, J. M. Gómez-Rodríguez, J. Colchero, J. Gómez-Herrero and A. M. Baro, *Rev. Sci. Instrum.*, 2007, **78**, 013705.
- L. G. Parratt, *Phys. Rev.*, 1954, **95**, 359–369.
- S. Hazra, A. Gibaud, A. Désert, V. Gacem and N. Cowlam, *Physica B*, 2000, **283**, 45–48.
- M. K. Bera, M. K. Sanyal, S. Pal, J. Daillant, A. Datta, G. U. Kulkarni, D. Luzet and O. Kononov, *Europhys. Lett.*, 2007, **78**, 56003.
- H. C. Hamaker, *Physica*, 1937, **4**, 1058–1072.

- 50 P. C. Ohara, D. V. Leff, J. R. Heath and W. M. Gelbart, *Phys. Rev. Lett.*, 1995, **75**, 3466–3469.
- 51 D. G. Schultz, X.-M. Lin, D. Li, J. Gebhardt, M. Meron, P. J. Viccaro and B. Lin, *J. Phys. Chem. B*, 2006, **110**, 24522–24529.
- 52 M. A. Boles, M. Engel and D. V. Talapin, *Chem. Rev.*, 2016, **116**, 11220–11289.
- 53 G. J. Kluth, M. M. Sung and R. Maboudian, *Langmuir*, 1997, **13**, 3775–3780.
- 54 J. K. Bal, S. Kundu and S. Hazra, *Chem. Phys. Lett.*, 2010, **500**, 90–95.
- 55 J. Drelich, E. Chibowski, D. D. Meng and K. Terpilowski, *Soft Matter*, 2011, **7**, 9804–9828.